between the passband peaks with successive diffraction orders was 33GHz and the full width at half maximum of the transmission band was 1.1GHz. This means that we can construct an optical spectrum analyser the resolution of which is 1.1GHz, or 8.8pm at 1.55μm by using the phase-compensated AWG.

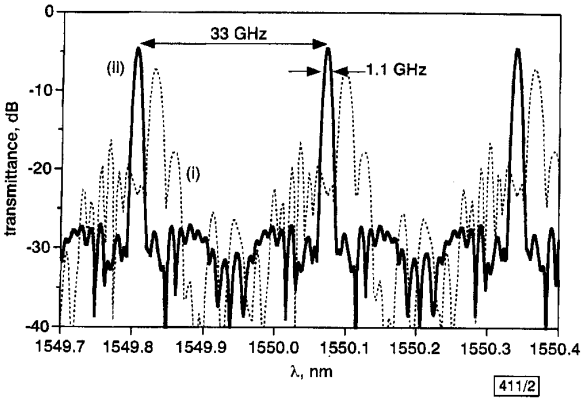

Fig. 2 *Transmission spectra for TE mode of 2GHz-spaced AWG*

Spectral resolution was 0.22GHz
(i) before compensation
(ii) after compensation

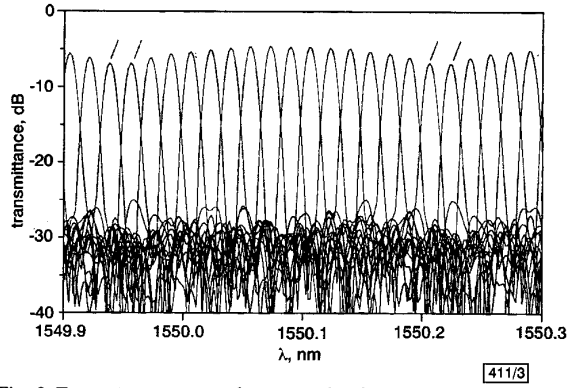

Fig. 3 *Transmission spectra for TE mode of 16 channels (1, 2, 16) of phase-compensated 2GHz-spaced AWG*

Fig. 3 shows the demultiplexing characteristics of all 16 channels for the TE mode of our phase-compensated AWG. Each channel was separated with a 2.1GHz spacing and the sidelobe components changed between –23 and –20dB as the output ports changed. The loss at the individual passband centres ranged between 4.5 and 6.8dB. Since the diffraction order was very large and the cyclic condition was satisfied [2], all the passbands that are obtained from the 16 output ports of the AWG with different diffraction orders are considered to arrange at 2.1GHz intervals in the 1.5μm band.

Conclusion: We have proposed a new configuration that enables fabrication of a 2GHz-spaced AWG demultiplexer. Since the path of each arrayed waveguide wound back and forth across the wafer without crossing any other waveguides, the whole waveguide pattern was contained on a 4-inch wafer. Although the fabricated AWG had phase errors of 20 radians, photosensitive phase compensation reduced the crosstalk values of all 16 channels to –23 to –20dB. By connecting the phase-compensated AWG to a parent AWG, we will be able to construct an integrated optical spectrum analyser with an 8.8pm spectral resolution for use as an optical frequency-monitoring instrument for DWDM networks.

26 July 2000
Electronics Letters Online No: 20001149
DOI: 10.1049/el:20001149

K. Takada, M. Abe, Y. Hida, T. Shibata, M. Ishii, A. Himeno and K. Okamoto (*NTT Photonics Laboratories, Tokai, Naka-gun, Ibaraki-ken, 319-1193, Japan*)

E-mail: takada@iba.iecl.ntt.oo.jp

References

1 TESHIMA, M., KOGA, M., and SATO, K.: 'Performance of multiwavelength simultaneous monitoring circuit employing arrayed-waveguide grating', *J. Lightwave Technol.*, 1996, **14**, pp. 2277–2285

2 TAKADA, K., YAMADA, H., and OKAMOTO, K.: 'Optical spectrum analyzer using cascaded AWGs with different channel spacings', *Photonics Technol. Lett.*, 1999, **11**, pp. 863–864

3 TAKAHASHI, H., SUZUKI, S., KATO, K., and NISHI, I.: 'Arrayed-waveguide grating for wavelength division multi/demultiplexer with nanometer resolution', *Electron. Lett.*, 1990, **26**, pp. 87–88

4 TAKADA, K., TANAKA, T., ABE, M., YANAGISAWA, T., ISHII, M., and OKAMOTO, K.: 'Beam-adjustment-free crosstalk reduction in 10GHz-spaced arrayed-waveguide grating via photosensitivity under UV laser irradiation through metal mask', *Electron. Lett.*, 2000, **36**, pp. 60–61

Time-lens-based spectral analysis of optical pulses by electrooptic phase modulation

N.K. Berger, B. Levit, S. Atkins and B. Fischer

The authors present a first experimental demonstration of time-lens-based operation by electrooptic phase modulation to perform real-time spectral analysis of optical pulse trains. The obtained resolution was 0.04nm. Under certain conditions the resolution of the real-time spectrum analyser can exceed that of conventional optical spectrum analysers.

Introduction and operation principle: Real-time spectrum analysis is based on performing Fourier transform of the input signal so that its spectrum is represented in the temporal envelope of the output signal [1]. Real-time Fourier transform processors were developed in radio frequencies for radar, sonar and communication systems using the chirp transform [2]. A simple way to perform a Fourier transform is to propagate the input signal through a delay line with quadratic dispersion. This method was utilised for far-infrared laser pulses using a dispersive delay line with surface acoustic waves [3]. For optical frequencies, it is possible to use a single-mode optical fibre [4, 5] or a chirped fibre grating [6, 7] as the dispersive delay line.

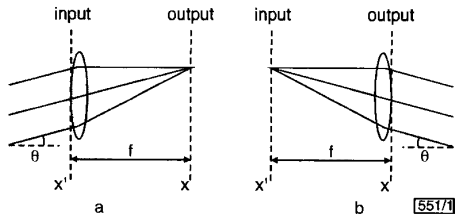

Fig. 1 *Spatial analogy of temporal operations used in this Letter*

a Spectral analysis
b Light envelope (shape) analysis

The analogy between propagation of pulses with narrow bandwidth in a dispersive medium and beam propagation in the paraxial diffraction regime is well known [1, 8]. On this basis, real-time spectrum operation using a dispersive delay line is analogous to Fourier transform of a spatial signal by Fraunhofer diffraction. The condition for having Fraunhofer diffraction in the time domain is given by $L \gg \tau_0^2/2\pi|\beta_2|$, where L is the length of delay line, τ_0 is the input pulse duration, $\beta_2 = d(1/v_g)/d\omega$ is the group velocity dispersion of the fibre, and ω is the light frequency. Under this condition, the output pulse width is $\tau = |D|L\Delta\lambda$, where $D = -2\pi c\beta_2/\lambda_0^2$, λ_0 and $\Delta\lambda$ are the central wavelength and the spectrum width of the input pulse, respectively, and c is the speed of light in vacuum. It is clear that the output pulse cannot be broader than the pulse period. These conditions significantly limit the corresponding relationships between the length of the delay line, the repetition rate and the spectrum width of the analysed pulses. To minimise these limitations it is possible to use a lens. In the spatial case (see Fig. 1*a*) each spatial spectral component,

defined by the angle θ, corresponds to a certain point in the focal plane. In the temporal case, a 'time lens' operation can be performed by using electrooptic phase modulation [8] or by mixing the original pulse with a chirped pulse in a nonlinear crystal [9]. The required phase modulation amplitude for measurement in the 'focal plane' of the time lens is $A = 2\pi c/\lambda_0^2\omega_m^2|D|L$, where ω_m is the frequency of the phase modulation. Under this condition, the envelope of the output signal provides the spectrum of the input pulse and a certain time t corresponds to a wavelength of the measured spectrum, $\lambda - \lambda_0 = t/DL$. In this Letter, real-time spectral analysis is realised using a dispersion compensating fibre as a dispersive delay line and an $LiNbO_3$ electrooptic phase modulator that gives the time-lens operation.

Experiments and results: In the first experiment, the optical pulses were generated using a mode-locked laser diode. The total dispersion of the delay line was $DL = -223$ps/nm. The delay between the optical pulse and the sine-wave voltage of the modulator was controlled by a phase-shifter. The optical spectrum of the input pulses was measured by a conventional commercial grating-based optical spectrum analyser, while the output pulses formed by our real-time spectrum analyser were measured using a fast photodetector and a sampling oscilloscope (both with a bandwidth of 50GHz). A comparison between these two spectra is shown in Fig. 2. The frequency of the laser pulse and the phase modulation was 6.12GHz, and the laser pulse duration was 29ps. The phase modulation amplitude was $A = 2.4$rad. The agreement between the two curves in Fig. 2 is good. The maximum discrepancy is ~0.02nm.

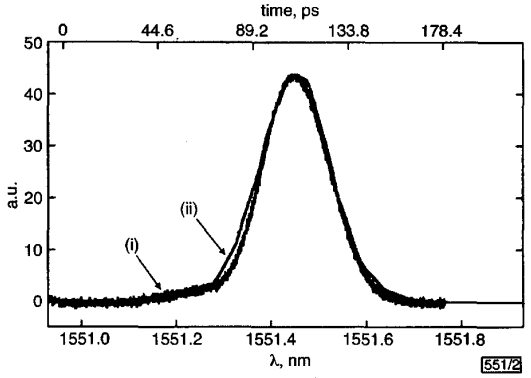

Fig. 2 *Spectrum of pulses from mode-locked laser diode given by proposed technique and conventional spectrum analyser*

(i) proposed technique (oscilloscope trace)
(ii) conventional spectrum analyser

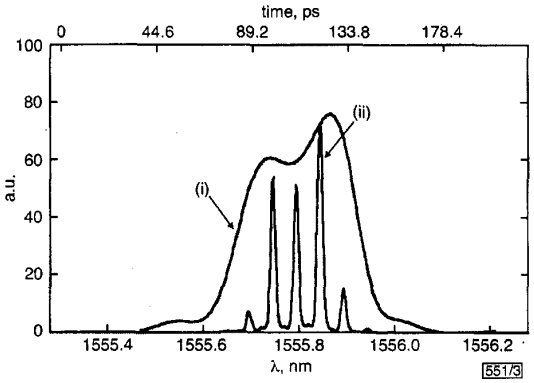

Fig. 3 *Spectrum of pulses generated by CW laser with phase modulator and propagation in a fibre given by proposed technique and conventional spectrum analyser*

(i) proposed technique (oscilloscope trace)
(ii) conventional spectrum analyser

In the second experiment, the input optical pulses were generated by propagating CW radiation of a tunable semiconductor laser through an electrooptic phase modulator [10] and a single-mode optical fibre with total dispersion of $DL = 416$ps/nm. The spectrum of the pulses measured by the conventional optical spectrum analyser and the output signal of our real-time spectrum analyser are shown in Fig. 3. In this case, the resolution of the optical spectrum analyser of 0.01nm was sufficient to resolve the discrete spectrum caused by the pulse periodicity. However, the time lens 'focuses' each pulse separately. Therefore our spectrum analyser records the spectrum of a single pulse or, in other words, the envelope of the spectrum of periodic pulses. In Fig. 3 we see that the maximum difference between the oscilloscope trace and the discrete spectrum envelope, e.g. for the location of the maxima, is < 0.02nm.

Our system can be modified as shown for the space analogy in Fig. 1*b*. Each point in the input plane x' of the spatial signal corresponds to a certain spectral component in the output plane x. In the time domain this means that a measurement of the pulse spectrum at the time-lens output makes it possible to determine the temporal structure of the input pulses [11] or their delay time [12]. In our third experiment, the time lens and the delay line were interchanged. Fig. 4 contrasts the oscilloscope trace of the input pulses and the spectrum measured at the output of the time lens by a commercial analyser, showing a good agreement with a discrepancy that does not exceed 2ps in most of the pulse trace.

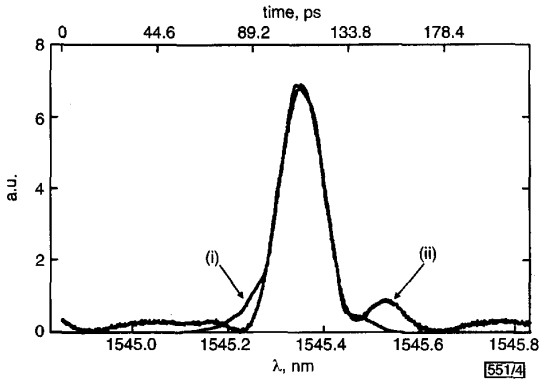

Fig. 4 *Pulse shape of CW laser with phase modulator and propagation in fibre given by proposed technique and conventional spectrum analyser*

(i) proposed technique (conventional spectrum analyser)
(ii) a direct time domain oscilloscope measurement

Discussion and conclusion: The errors in our method can originate from several sources: non-quadracity of the dispersion, non-parabolity of the phase modulation, the finite 'aperture' of the time lens, and the time response of the detector and the oscilloscope. The resolution in our experiment is estimated to be ~0.04nm. However, shorter pulses with lower repetition rate and higher dispersion lines provide better accuracy, e.g. for 5ps pulses with 1.4GHz repetition rate $A = 44$rad [10] and $DL = 223$ps/nm, the resolution is ~0.005nm. Thus, under certain conditions the resolution of real-time spectrum analyser can exceed that of present commercial optical spectrum analysers.

Acknowledgment: We acknowledge the support of the Israel Ministry of Science and the European Community in the fifth frame under the METEOR Project.

1 August 2000
Electronics Letters Online No: 20001174
DOI: 10.1049/el:20001174

N.K. Berger, B. Levit, S. Atkins and B. Fischer (*Department of Electrical Engineering, Technion – Israel Institute of Technology, Technion City, Haifa 32000, Israel*)

E-mail: fischer@ee.technion.ac.il

References

1 PAPOULIS, A.: 'Pulse compression, fibre communications, and diffraction: a unified approach', *J. Opt. Soc. Am. A*, 1994, **11**, (1), pp. 3–13

2 JACK, M.A., GRANT, P.M., and COLLINS, J.H.: 'The theory, design, and applications of surface acoustic wave Fourier-transform processors', *Proc. IEEE*, 1980, **68**, (4), pp. 450–468

3 FETTERMAN, H.R., TANNENWALD, P.E., PARKER, C.D., MELNGAILIS, J., WILLIAMSON, R.C., WOSKOBOINIKOW, P., PRADDAUDE, H.C., and MULLIGAN, W.J.: 'Real-time spectral analysis of far-infrared laser pulses using a SAW dispersive delay line', *Appl. Phys. Lett.*, 1979, **34**, (2), pp. 123–125
4 TONG, Y.C., CHAN, L.Y., and TSANG, H.K.: 'Fibre dispersion or pulse spectrum measurement using a sampling oscilloscope', *Electron. Lett.*, 1997, **33**, (11), pp. 983–985
5 KELKAR, P.V., COPPINGER, F., BHUSHAN, A.S., and JALALY, B.: 'Time-domain optical sensing', *Electron. Lett.*, 1999, **35**, (19), pp. 1661–1662
6 MURIEL, M.A., AZAÑA, J., and CARBALLAR, A.: 'Real-time Fourier transformer based on fibre gratings', *Opt. Lett.*, 1999, **24**, (1), pp. 1–3
7 BERGER, N.K., LEVIT, B., BEKKER, A., and FISCHER, B.: 'Real-time optical spectrum analyser based on chirped fibre Bragg gratings', *Electron. Lett.*, 2000, **36**, (14), pp. 1189–1191
8 KOLNER, B.H.: 'Space-time duality and the theory of temporal imaging', *IEEE J. Quantum Electron.*, 1994, **30**, (8), pp. 1951–1963
9 BENNETT, C.V., and KOLNER, B.H.: 'Upconversion time microscope demonstrating 103× magnification of femtosecond waveforms', *Opt. Lett.*, 1999, **24**, (11), pp. 783–785
10 GODIL, A.A., AULD, B.A., and BLOOM, D.M.: 'Picosecond time-lenses', *IEEE J. Quantum Electron.*, 1994, **30**, (3), pp. 827–837
11 KAUFFMAN, M.T., BANYAI, W.C., GODIL, A.A., and BLOOM, D.M.: 'Time-to-frequency converter for measuring picosecond optical pulses', *Appl. Phys. Lett.*, 1994, **64**, (3), pp. 270–272
12 ARONS, E., LEITH, E.N., TIEN, A., and WAGNER, R.: 'High resolution optical chirped pulse gating', *Appl. Opt.*, 1997, **36**, (12), pp. 2603–2608

Description of dual frequency polarimetric data using Gell-Mann parameter set

L. Ferro-Famil and E. Pottier

A method to describe dual frequency polarimetric images by determining the rigorous change in polarisation between both data sets is presented. The variation in the backscattered wave polarisation properties is parameterised in terms of eight real Gell-Mann coefficients. This method is applied on dual frequency polarimetric synthetic aperture radar data.

Introduction: The polarimetric properties of the response of a natural medium to an incident electromagnetic wave are highly linked to its intrinsic physical characteristics and relate to the underlying scattering mechanism [1]. The use of dual frequency polarimetric data sets has been shown to increase in an important way the analysis and inversion capabilities in quantitative remote sensing of natural media [2]. For dual frequency measurements, the ratio of the size of a scatterer with respect to the incident wavelength is a critical parameter which conditions the nature of the scattering mechanism. Inversion algorithms are usually based on the separate observations and interpretations of scattering terms. In this Letter we propose that dual frequency polarimetric synthetic aperture radar (SAR) data can be described by identifying the rigorous full polarimetric variation from one data set to the other. The variation is summarised into eight real coefficients obtained from special unitary operator transformation analysis.

Special unitary transformation: By means of a projection on the Pauli spin matrix set, a scattering matrix $\mathbf{S}$ transforms, in the monostatic case, to a complex target vector $\mathbf{k}$ used to define a coherency matrix $\mathbf{T}$ as follows:

$$\mathbf{T} = \mathbf{k}\mathbf{k}^H \text{ with } \mathbf{k} = \frac{1}{\sqrt{2}}[S_{HH}+S_{VV}, S_{HH}-S_{VV}, 2S_{HV}]^T \quad (1)$$

The (3 × 3) coherency matrix $\mathbf{T}$ has rank one and can be expressed as follows:

$$\mathbf{T} = \lambda(\mathbf{V}\Sigma_0\mathbf{V}^{-1}) = \lambda\mathbf{u}\mathbf{u}^H \text{ with } \Sigma_0 = \text{diag}[1\ 0\ 0] \quad (2)$$

where Σ_0 and $\mathbf{V}$ represent respectively the eigenvalue and eigenvector matrices of $\mathbf{T}$. $\mathbf{u}$ is the unitary eigenvector related to the single nonzero eigenvalue λ, and represents the normalised target vector. It may be expressed as a function of five real variables as

$$\mathbf{u} = [\cos\alpha e^{j\xi}, \sin\alpha\cos\beta e^{j\delta}, \sin\alpha\sin\beta e^{j\gamma}]^T \quad (3)$$

These variables were shown to be highly related to the physical properties of the observed medium [1]. The constant structure of the eigenvalue matrix requires that coherency matrices measured at different frequencies $\mathbf{T}_1$ and $\mathbf{T}_2$ present normalised target vectors, $\mathbf{u}_1$ and $\mathbf{u}_2$, which are linked by way of a special unitary transformation as shown in eqn. 4,

$$\mathbf{V}_2\Sigma_0\mathbf{V}_2^{-1} = \mathbf{U}_3(\mathbf{V}_1\Sigma_0\mathbf{V}_1^{-1})\mathbf{U}_3^{-1} \Rightarrow \mathbf{u}_2 = \mathbf{U}_3\mathbf{u}_1 \quad (4)$$

where $\mathbf{U}_3$ is a (3 × 3) complex special unitary operator which verifies $\mathbf{U}_3^H = \mathbf{U}_3^{-1}$ and $\det(\mathbf{U}_3) = +1$. The operator $\mathbf{U}_3$ completely defines the change of scattering basis from $\mathbf{T}_1$ to $\mathbf{T}_2$, and then summarises the modification in the scattering mechanism as the observation frequency varies.

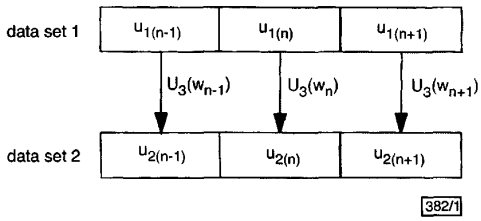

Fig. 1 *Special unitary transformations between successive dual frequency samples*

Full polarimetric variation parameterisation: To describe the change in polarimetric properties, $\mathbf{U}_3$ is decomposed into parameters which may lead to a physical interpretation. As an element of the special unitary group (SU3), $\mathbf{U}_3$ is expressed in terms of a matrix complex exponential of a linear combination of the eight traceless and hermitian Gell-Mann matrices:

$$\mathbf{U}_3 = \exp\left(j\sum_{i=1}^{8} w_i\mathbf{G}_i\right) \quad (5)$$

where w_i represents a real angular variable, $-\pi \le w_i \le \pi$, and $\mathbf{G}_i$ the corresponding Gell-Mann set generator. Any element of SU3 is exactly defined by its real weighting vector $\mathbf{w} = [w_1, ..., w_8]$. Determination of $\mathbf{w}$ is achieved by solving the nonlinear equation set $\mathbf{u}_2 = \mathbf{U}_3(\mathbf{w})\mathbf{u}_1$. This under-determined system of five equations in eight unknowns leads to an infinite number of solutions [3]. A practical method to extract the Gell-Mann parameter vector $\mathbf{w}$ consists of assuming that the polarimetric variation from one data set to the other remains constant over two sample periods, i.e. $\mathbf{U}_3(\mathbf{w}_n) \simeq \mathbf{U}_3(\mathbf{w}_{n+1})$ in Fig. 1.

The resolution of the resulting over-determined set of equations is performed by a least squares nonlinear optimisation technique to determine $\mathbf{w}$, which minimises the real scalar ε^2 as shown in eqn. 6,

$$\varepsilon^2(\mathbf{w}) = \mathbf{K}^H\mathbf{K} \text{ with } \mathbf{K} = \begin{bmatrix} \mathbf{u}_{2n} - \mathbf{U}_3(\mathbf{w})\mathbf{u}_{1n} \\ \mathbf{u}_{2(n+1)} - \mathbf{U}_3(\mathbf{w})\mathbf{u}_{1(n+1)} \end{bmatrix} \quad (6)$$

Results: This method was applied using polarimetric SAR data acquired by a NASA/JPL AirSAR sensor over the Nezer Forest in France in 1989, at both P and L frequency bands, corresponding respectively to 0.44GHz and 1.225GHz. The data sets represent a column of 900 samples of the polarimetric images. Fig. 2 shows the co-polarisation scattering coefficients $|S_{HH}|$ and $|S_{VV}|$ normalised with respect to the total polarimetric power at both P and L bands. The vertical dotted lines represent the separations between the different forest parcels discriminated along the range direction. The polarimetric scattering coefficients from both data sets do not allow the forest parcel distribution over the samples to be retrieved directly. The SU3 operator parameterisation with the eight real Gell-Mann coefficients is processed using the 900 samples, using the Levenberg-Marquardt nonlinear optimisation method to solve eqn. 6. The simultaneous observation of two of the eight parameters, w_1 and w_3, presented in Fig. 3, clearly shows the change in polarimetric information from P band to L band